Hybrid stars in an SU(3) parity doublet model

V. Dexheimer[*]

Department of Physics, Kent State University, Kent OH, USA

J. Steinheimer[†]

Lawrence Berkeley National Laboratory, 1 Cyclotron Road, Berkeley, California 94720, USA and
FIAS, Johann Wolfgang Goethe University, Frankfurt am Main, Germany

R. Negreiros[‡]

Physics Department, Universidade Federal Fluminense, Niterói, Brazil and
FIAS, Johann Wolfgang Goethe University, Frankfurt am Main, Germany

S. Schramm[§]

FIAS, Johann Wolfgang Goethe University, Frankfurt am Main, Germany

We apply an extended version of the SU(3) parity model, containing quark degrees of freedom, to study neutron stars. The model successfully reproduces the main thermodynamic features of QCD which allows us to describe the composition of dense matter. Chiral symmetry restoration is realized inside the star and the chiral partners of the baryons appear, their masses becoming degenerate. Furthermore, quark degrees of freedom appear in a transition to a deconfined state. Performing an investigation of the macroscopic properties of neutron stars, we show that observational constraints, such as mass and thermal evolution, are satisfied and new predictions can be made.

I. INTRODUCTION

The study of strong interaction physics under extreme conditions is a central topic of nuclear physics, with a large number of experimental and theoretical programs focusing on the area. These conditions comprise large temperatures, densities, as well as extreme values of nuclear isospin. In ultrarelativistic heavy-ion collisions a very hot fireball is created in the collision zone and, at high temperatures, hadronic matter is assumed to melt into its constituents, quarks and gluons. The net baryon density in such reactions is determined by the beam energy. At the planned energies in the upcoming FAIR (Facility for Antiproton and Ion Research) at GSI, a hot and relatively dense system will be produced. A central point of these investigations is the understanding of the quark-hadron phase transition. However, while relatively high densities and finite temperatures might be reached in laboratory experiments, the study of neutron stars is essential if one wants to probe the low temperature and high density region of the phase diagram of strongly interacting matter.

Observations of neutron star masses (and possibly radii) provide the standard way of constraining the inner composition of these objects. More precisely, recent observations have set new high mass constraints for neutron stars (PSR J1614-2230 [1] being the most important), and equations of state aimed

to describe compact stars are thus expected to provide objects with high masses [2–6]. In the case of hybrid stars (neutron stars with a quark core in its center), a quark phase based on a simple noninteracting quark model such as the MIT bag model tends to reduce the maximum mass significantly (see the discussion in Ref. [7]). A quark phase that includes strong repulsive interactions, however, may have an equation of state quite similar to a purely hadronic one. This prevents the softening of the matter and the drop in maximum mass [8–10]. It has been found, however, that models with a strong repulsive quark-quark interaction make the description of lattice results at $\mu_B = 0$ nearly impossible [11–13], since including a repulsive mean field interaction decreases the quark number susceptibility. Therefore, most current successful hybrid star models would fail in this regard if they were to be applied to the high-temperature, low-density regime.

At high temperatures, QCD exhibits a crossover to a deconfined phase and the quarks and gluons become the dominant degrees of freedom [14]. The temperature at which this transition takes place is estimated to be $T_{\text{dec}} \approx 150$–160 MeV [15,16]. A phase transition is also expected to take place at high densities, where baryons start to overlap, and quarks and gluons become the effective degrees of freedom. This indicates that at some point a hadronic model will not be able to appropriately describe the matter present inside a neutron star, and a deconfinement mechanism needs to be introduced.

In the following, we will discuss a theoretical approach that is able to describe the conditions found in compact stars as well as those created in heavy-ion collisions. The aim of this approach is to find a unified description for the thermodynamic properties of QCD which can be applied to compact stars and

———————
[*]vdexheim@kent.edu
[†]JSFroschauer@lbl.gov
[‡]negreiros@fias.uni-frankfurt.de
[§]schramm@fias.uni-frankfurt.de

heavy-ion collisions at different beam energies while being in accordance with lattice QCD results at vanishing baryon density. An approach of this type is essential if one wants to investigate a phase diagram that has a region of a crossover transition to quark matter (as is clearly established by lattice QCD calculations) and a first-order transition at high densities and low temperatures. This is not possible by combining separate models for the hadronic and quark phases. Such a first-order transition at low temperature has also been observed in recent lattice Monte Carlo calculations of an effective QCD Lagrangian [17]. In addition, a model that can cover the physics at high temperature as well as at high density can serve as an important tool for the increasingly important studies of black-hole formation and black-hole neutron-star mergers, where temperatures up to 90 MeV and high densities might be reached [18,19].

In a previous paper, an extended quark $SU(3)_f$ parity doublet model was introduced for this purpose [20]. In the parity model [21,22], the mass splitting between the nucleons and the respective chiral partners is generated by the spontaneous breaking of chiral symmetry and their coupling to the corresponding order parameter, the scalar (sigma) field. The same applies for the baryon octet in the $SU(3)_f$ case [23,24]. When chiral symmetry is restored and the sigma field vanishes, the chiral partner masses become degenerate. A good description of nuclear saturation properties, as well as neutron star observables, can easily be achieved within this formalism [25,26]. In Ref. [27] a phase diagram for chiral symmetry restoration was calculated using an $SU(2)_f$ version of the parity model.

In addition, the parity model has been shown to describe the lattice results at $\mu_B = 0$ and can be used in dynamical models for relativistic heavy-ion collisions [28–30]. We will apply this model to the study of neutron stars. A complete phase diagram for isospin symmetric matter, using the extended version of the $SU(3)_f$ parity model, which contains quark degrees of freedom, has been calculated in Ref. [20]. As expected, at low temperatures the nuclear matter liquid-gas phase transition and the chiral symmetry restoration are of first order. Within this approach the deconfinement phase transition, on the other hand, is a crossover. Furthermore, chiral symmetry restoration and deconfinement do not coincide, and at intermediate densities the matter is chirally symmetric but still confined. Whether such a chirally symmetric hadronic phase can be the $N_c = 3$ equivalent of the $N_c = \infty$ quarkyonic phase [31] is still subject to debate [32–34].

In this paper we investigate the properties of electrically-neutral chemically equilibrated matter in the framework of the model described above. We will investigate the influence of the chiral partners, hyperons, and quark matter on the macroscopic properties of a neutron star, such as its gravitational mass, radius, and thermal evolution.

II. THE SU(3) PARITY DOUBLET MODEL

Considering that the baryons are grouped in doublets (B_+ and B_-), in which they belong to the same multiplet, the components of the fields ψ_1 and ψ_2 transform under L and

R rotations as

$$\psi'_{1R} = R\psi_{1R}, \quad \psi'_{1L} = L\psi_{1L},$$
$$\psi'_{2R} = L\psi_{2R}, \quad \psi'_{2L} = R\psi_{2L}. \quad (1)$$

This formalism allows the presence of a bare mass term in the Lagrangian density that does not break chiral symmetry,

$$m_0(\bar{\psi}_2\gamma_5\psi_1 - \bar{\psi}_1\gamma_5\psi_2)$$
$$= m_0(\bar{\psi}_{2L}\psi_{1R} - \bar{\psi}_{2R}\psi_{1L} - \bar{\psi}_{1L}\psi_{2R} + \bar{\psi}_{1R}\psi_{2L}), \quad (2)$$

where m_0 represents a mass parameter. Since the term proportional to m_0 mixes the upper and lower components of the parity doublets, one diagonalizes the matrix by introducing new fields B with a diagonal mass matrix. Keeping only the diagonal meson contributions, the scalar and vector condensates in the mean field approximation, the resulting Lagrangian reads

$$\mathcal{L}_B = \sum_i (\bar{B}_i i \slashed{\partial} B_i) + \sum_i (\bar{B}_i m_i^* B_i)$$
$$+ \sum_i [\bar{B}_i \gamma_\mu (g_{\omega i}\omega^\mu + g_{\rho i}\rho^\mu + g_{\phi i}\phi^\mu) B_i], \quad (3)$$

where the coupling constants for the baryons with the mesons ω, ρ and the strange meson ϕ are $g_{B\omega}$, $g_{B\rho}$, and $g_{B\phi}$, respectively. We do not include a vector-meson self-interaction to avoid an extra softening of the equation of state, which in turn would yield neutron stars with very low maximum mass [26,35]. This happens because, as the coupling constant increases, the respective vector-isoscalar field decreases (in order to reproduce saturation properties), thus making the repulsive part of the strong force less pronounced.

The expression for the effective masses of the baryons for isospin symmetric matter reads

$$m_i^* = \sqrt{\left[\left(g_{\sigma i}^{(1)}\sigma + g_{\zeta i}^{(1)}\zeta\right)^2 + (m_0 + n_s m_s)^2\right]}$$
$$\pm g_{\sigma i}^{(2)}\sigma \pm g_{\zeta i}^{(2)}\zeta. \quad (4)$$

In the above equation, the term that does not correspond to the bare mass is generated by the scalar mesons σ, the strange ζ, and by the SU(3)-breaking mass term with $m_s = 150$ MeV. The last term is responsible for the generation of an explicit mass corresponding to the strangeness n_s of the baryon. The values of the various coupling constants of the baryons with the meson fields are given in Ref. [20]. The couplings $g^{(2)}$ are chosen in order to reproduce the splitting of the masses of the parity partners in vacuum, further assuming, for simplicity, an equal splitting of the masses of the various baryonic doublets ($g_{\sigma i}^{(2)} = -0.850$, $g_{\zeta i}^{(2)} = 0$). The coupling constants $g_i^{(1)}$ are chosen in order to reproduce vacuum masses of baryons. The bare mass parameter is set to $m_0 = 810$ MeV. Such a high value is necessary in order to reproduce reasonably massive stars while keeping the compressibility of saturated matter at reasonable values [25,26]. The value for the strange quark mass m_s is fixed to 150 MeV.

The nucleonic vector interactions are tuned to reproduce reasonable values for the nuclear ground state properties (binding energy per baryon of $\sim$−16 MeV and baryonic density of $\rho_0 = 0.15$ fm^3 at saturation) while the hyperonic

vector interactions are tuned to generate reasonable optical potentials for the hyperons in ground state nuclear matter ($U_\Lambda \sim -28$ MeV, $U_\Sigma \sim -14.5$ MeV, and $U_\Xi \sim -18$ MeV). The equations of motion are obtained by minimizing the grand canonical potential (a function of baryonic chemical potential and temperature), and are solved self-consistently in mean field approximation. For nonzero temperature calculations, a hadronic heat bath is included.

We choose the vacuum mass of the chiral parter for the nucleons to be 1535 MeV, the lighter resonance with spin 1/2 and negative parity. Lower values for this mass ($\sim$1200 MeV for instance) would lead to chiral restoration taking place at lower densities [35], and to less massive stars [25]. In addition, using a formula for the width as a function of the bare mass parameter m_0 [21], one finds that the width of the less massive resonance would be too small to have escaped experimental detection [26]. Other candidates such as 1650 MeV also have been suggested [36]. For the hyperons, we simply chose the splitting between the particles and the respective parity partners to have the same value as for the nucleons, thus keeping the number of parameters to a minimum. This assumption agrees quite well with some parity partner candidates, such as the $\Lambda(1670)$ and the $\Sigma(1750)$. In the case of the Ξ the data is unclear.

III. INCLUSION OF QUARKS

Following [20], the effective masses of the quarks are generated by the scalar mesons except for a small explicit mass term ($\delta m_q = 5$ MeV and $\delta m_s = 150$ MeV for the strange quark) and m_{0_q}

$$m_q^* = g_{q\sigma}\sigma + \delta m_q + m_{0q}, \quad m_s^* = g_{s\zeta}\zeta + \delta m_s + m_{0q}, \tag{5}$$

with $g_{q\sigma} = g_{s\zeta} = 4.0$. As was the case for baryons, we have also introduced a mass parameter $m_{0q} = 200$ MeV for the quarks.

We use the Polyakov loop Φ as the order parameter for deconfinement. The field Φ is defined via $\Phi = \frac{1}{3}\text{Tr}[\exp(i \int d\tau A_4)]$, where $A_4 = iA_0$ is the temporal component of the SU(3) gauge field [37–39]. The coupling of the quarks to the Polyakov loop is introduced in the thermal energy of the quarks (see Ref. [20] for more details). All thermodynamical quantities are derived from the grand canonical potential that includes the effective potential $U(\Phi, \Phi^*, T)$, which controls the dynamics of the Polyakov loop. In our approach we adopt the ansatz proposed in Refs. [40,41],

$$U = -\frac{1}{2}a(T)\Phi\Phi^*$$
$$+ b(T)\ln[1 - 6\Phi\Phi^* + 4(\Phi^3\Phi^{*3}) - 3(\Phi\Phi^*)^2], \tag{6}$$

with $a(T) = a_0 T^4 + a_1 T_0 T^3 + a_2 T_0^2 T^2$ and $b(T) = b_3 T_0^3 T$. The parameters are fixed, as in Ref. [40], by demanding a first-order phase transition in the pure gauge sector at $T_0 = 270$ MeV, and that the Stefan-Boltzmann limit of a gas of gluons is reached for $T \to \infty$.

To remove the hadronic contributions from the equation of state at high temperatures and densities, we introduce

excluded volume effects. The inclusion of finite-volume effects in thermodynamic models for hadronic matter was proposed in Refs. [43–55]. In recent publications [20,56] we adopted this ansatz to successfully describe a smooth transition from a hadronic to a quark dominated system. The modified chemical potential $\widetilde{\mu}_i$, which is connected to the real chemical potential μ_i of the ith particle species, is obtained by the relation

$$\widetilde{\mu}_i = \mu_i - v_i P, \tag{7}$$

where $v_i = 1$ fm^3 is the excluded volume of a particle of species i (zero for quarks), and P is the sum over all partial pressures. To be thermodynamically consistent, all densities (energy density $\widetilde{e}_i$, baryon density $\widetilde{\rho}_i$, and entropy density $\widetilde{s}_i$) were multiplied by a volume correction factor f, which is the ratio of the total volume V and the reduced volume V' not being occupied. As a consequence, the chemical potentials of the hadrons are decreased by the quarks, but not vice versa. In other words, as the quarks start appearing, they effectively suppress the hadrons by changing their chemical potential, while the quarks are only affected through the volume correction factor f.

A shortcoming of the parametrization above is that the compressibility of bulk matter at saturation density is too high (525 MeV) and the equations of state is a bit too stiff a low densities when compared with heavy-ion collision data from Ref. [57]. For this reason, in addition to the parametrization discussed above (model A hereafter), we use a second parametrization (model B) that leads to more realistic values for the compressibility ($\kappa \approx 330$ MeV). The values of the modified parameters in model B are $v_i = 0.5$ fm^3, $g_{N\omega} = 5.02$, $g_\sigma^{(1)} = -7.79$, and $g_\sigma^{(2)} = -0.76$ (see Table I of Ref. [20] for the entire parameter set). The symmetry energy obtained at saturation is 32.6 and 32.4 MeV and its slope L is 99 and 92 MeV, respectively, for models A and B. Both of these are in reasonable agreement with symmetry energy constraints from Ref. [58].

It is important to notice that, although v_i is directed related to the position of the phase transitions that occur when new particles appear in the system, it cannot be varied freely. This parameter is chosen mainly to reproduce lattice QCD results at $\mu_B = 0$ for model A. For model B, one has more freedom for the choice of v_i, but the phase transitions reproduced do not change qualitatively with this variation. This happens because, in this type of unified equation of state, the order in which the particles appear depends strongly on charge neutrality. For example, negatively charged particles, such as the down quark, will always be favored with respect to positive ones.

IV. RESULTS

By assuming chemical equilibrium and charge neutrality, we obtain an equation of state that describes neutron star matter. This, in turn, can be used to obtain a solution of the Tolman-Oppenheimer-Volkoff equation [59,60], which allows us to study how the system behaves under the influence of gravity. We show in Fig. 1 sequences of stars with gravitational mass M and radius R for models A and B. For model A, the maximum mass obtained for a cold star is $1.96M_\odot$, which is in
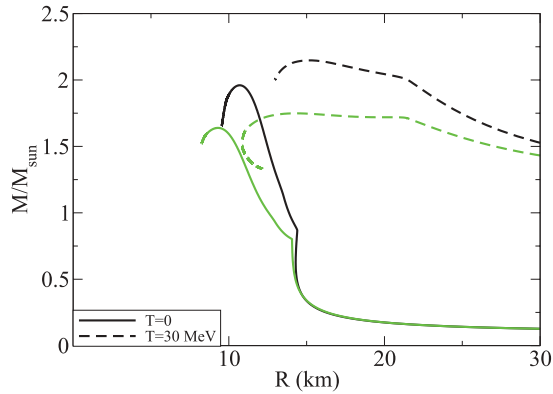
FIG. 1. (Color online) Mass-radius diagram for star families with different temperatures shown for models A and B (black and green lines, respectively). For the cold case we have included a cold crust from Ref. [42] and for the warm case we have included a crust with $s/\rho_B = 4$ in accordance with Ref. [43].
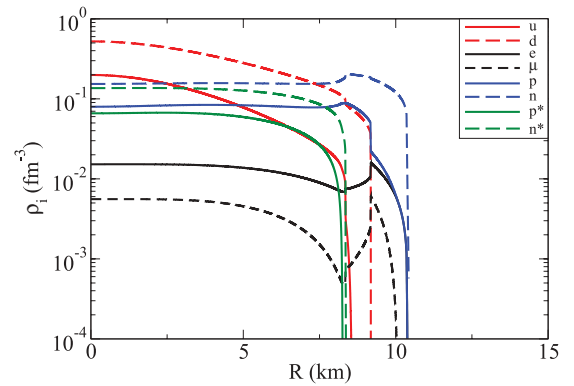

FIG. 2. (Color online) Population (particle density) as a function of star radius for a cold star using model A. Quark densities are divided by 3.

agreement with observations of J1614-2230 ($1.97 \pm 0.04 M_\odot$) [1]. For a star with a temperature of 30 MeV, corresponding to a proto-neutron star, the maximum mass obtained increases to $2.15 M_\odot$. The radius (corresponding to the most stable massive star) increases from 10.70 to 15.17 km, the central baryonic density decreases from 1.16 to 0.90 fm^{-3}, and the central fraction of quarks decreases from $\sim$60% to $\sim$50% when a warm star is considered.

As for model B, the maximum mass obtained for a cold star reduces to $1.64 M_\odot$. For a star with a temperature of 30 MeV the maximum mass obtained is $1.75 M_\odot$. The radius of the most stable massive star, in this case, increases from 9.30 to 14.28 km, the central baryonic density decreases from 1.58 to 1.18 fm^{-3}, and the central fraction of quarks decreases from $\sim$50% to $\sim$40% when a warm star is considered. We clearly see that the price paid to obtain a realistic compressibility is the reduction of the maximum mass of the neutron star. This effect is generally model independent, but is known to be more pronounced in the parity model. It is important to keep in mind that we have not included in the present calculation any rotational or strong magnetic field effects in order to keep the effect of the appearance of the parity partners more clear. Both rotation and strong magnetic fields are known to increase the maximum mass of neutron stars [61,62].

In principle, the correct quantity to be used in order to analyze proto-neutron star temporal evolution is the entropy per baryon, instead of the temperature. Besides, trapped neutrinos should be included in earlier stages of star evolution, when the temperature (or entropy per baryon) is higher. Although these features are of great interest, our goal in this preliminary study of the topic is to analyze the application of the model to neutron stars in the simplest case of $T = 0$ and the second simplest case of $T = 30$ MeV. Nevertheless, we chose 30 MeV for the finite-temperature case because it is approximately the maximum temperature reproduced in the center of neutron stars when the entropy per baryon is fixed to 2. In this way, we study the two limiting cases of the star evolution ($T = 0$ and $T = 30$ MeV). Nevertheless, one can see that if the baryon number has to remain constant (as in the case

of isolated stars) not all stars from Fig. 1 exist throughout the evolution, and some eventually collapse into black holes. For example, the maximum baryon number for parametrization A is 2.73×10^{57} at $T = 0$ and 2.92×10^{57} at $T = 30$, and for parametrization B it is 2.24×10^{57} at $T = 0$ and 2.32×10^{57} at $T = 30$. In a detailed study of the matter, all the considerations above have to be taken into account.

The particle population of the cold maximum mass neutron stars obtained by both models is shown in Figs. 2 and 3. We see that at low densities both stars consist only of neutrons, protons, electrons, and muons. Towards the center of the stars the quarks appear (first the d, followed by the u) followed by the chiral partners (of neutrons and protons). The threshold for the quarks to appear is $1.56\rho_0$ and $2.16\rho_0$ for parametrizations A and B, respectively. It is interesting to notice that in this model the baryons appear in small quantities but do not vanish at high densities. This is a consequence of the suppression of the hadrons due to the excluded volume prescription. The hadrons are suppressed exponentially by the quark pressure though not removed entirely. Note, however, that their fraction becomes so small that their contribution to the thermodynamics of the system is negligible. Furthermore, at high densities, the amount of nucleons and the respective chiral partners is very similar.
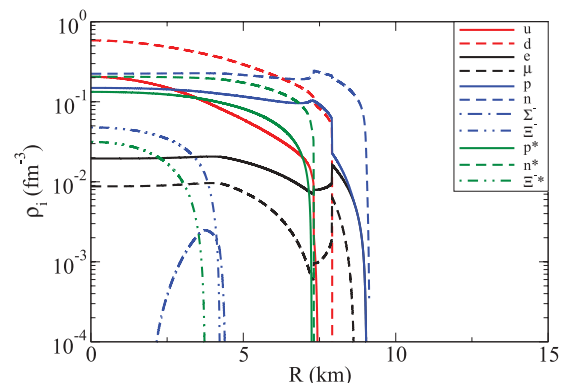

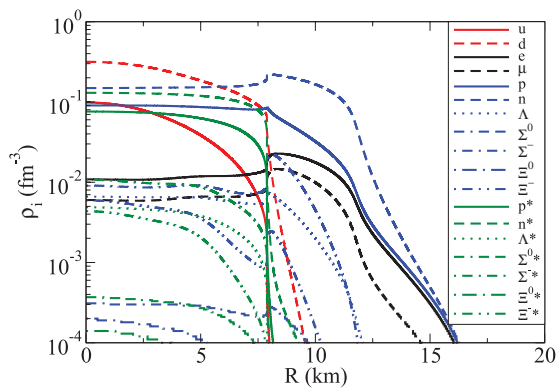FIG. 3. (Color online) Same as Fig. 2 but for model B.

FIG. 4. (Color online) Population (particle density) as a function of star radius for a warm star, $T = 30$ MeV, using model A. Quark densities are divided by 3.

FIG. 5. (Color online) Same as Fig. 4 but for model B.

Particles that contain strangeness, despite being included in the model, do not appear or appear in very small quantities in the cold stars. This is due their large bare masses and the slow restoration of the strange scalar (ζ) field to its zero value at high densities.

The decrease in central density stated above is not enough to prevent strange particles from appearing in the core of warm stars (Figs. 4 and 5). At low densities we see Λ's, Σ^-'s, Ξ^-'s, and Σ^0's, and at high densities Ξ^0's, all with their respective chiral partners. The strange quarks only appear at densities beyond the ones present in the studied stars. Overall, the amount of particles that contain strangeness is not high enough to significantly change star properties such as mass and radius. These properties are influenced mainly by the pressure and energy density changing substantially due to the high temperature, and the Polyakov potential U, which only affects the system at finite temperature.[1]

Note that the order of the appearance of the hyperons in the star does not happen simply according to their vacuum masses. Their appearance is related to the relation between their effective masses and their effective chemical potentials. At zero temperature, for example, a particle only appears when its effective chemical potential is larger than its effective mass. For finite temperature, thermal effects also contribute, making the above requirement more relaxed. But more importantly, the order of the particles in a star is strongly constrained by charged neutrality. This makes the appearance of negative charged hyperons more favorable, followed by charge neutral ones. Therefore, the only particles that appear in significant quantities for parametrization B at $T = 30$ MeV are the Σ^- followed by the Ξ^- and respective chiral partners and they are the ones that still appear at $T = 0$. For parametrization A, because there are no significant quantity of hyperons at $T = 30$ MeV, there are also no hyperons in the $T = 0$ MeV case.
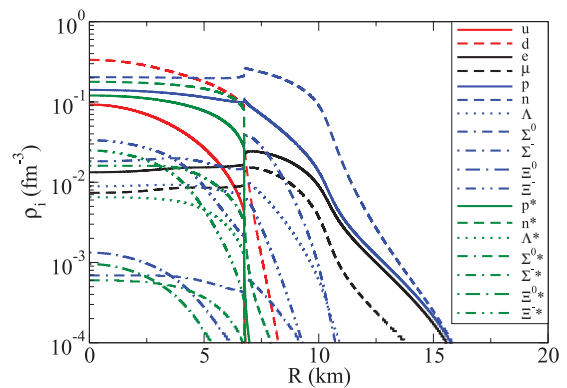
For the cold case, there are basically two first-order phase transitions in the star: when the down quarks appear and when the up quarks and chiral partners appear. For the warm case, both of these transitions are smoother and closer to each other. For the symmetric case, relevant for heavy-ion collisions, the phase transitions would be stronger for any temperature, since chemical equilibrium and charge neutrality push the chiral symmetry restoration (related to the appearance of chiral partners) to lower densities with respect to the symmetric matter case and render the transition smoother [26].

V. THERMAL EVOLUTION

The thermal evolution of the stars was obtained by solving the full set of equations that govern energy balance and transport in a relativistic star [64]. We have considered the standard neutrino emission processes for both quarks and hadrons; these are the direct Urca (DU), modified Urca (MU), and Bremsstrahlung (BM) processes [65,66]. The specific heat of the matter is given by the traditional specific heat of relativistic fermions, as described in Ref. [67]. The thermal conductivity is calculated as described in Refs. [68,69]. Finally, the boundary condition that defines the surface temperature of the star is discussed in Refs. [70–73]. In our calculations we assume a nonmagnetized surface, with an accreted envelope of $\Delta M/M = 1.0 \times 10^{-9}$.

We have also taken into account neutron superfluidity when calculating the thermal evolution. The pairing patterns considered were the neutron singlet ($^1S_0$) and triplet ($^3P_2$) states, as described in Refs. [74,75]. We point out that it is possible that protons form a singlet superconductor [76,77], however, the pairing of protons in the core is still not very well understood (see Ref. [78] and references therein). For that reason we consider only neutron superfluidity at this stage. We show in Figs. 6 and 7 the cooling of stars with different masses (for models A and B, respectively), T_∞ being the redshifted surface temperature. We also plot a set of prominent observed cooling data, where circles denote objects whose age was determined through spin-down, squares through the object motion with respect to originating supernova (kinematic age) [67,79], and diamonds show the evolution of Cas A [77]. We note that although our model exhibits temperatures and

---

[1]An example for a Polyakov potential for the deconfinement order parameter that also depends on baryon density, i.e., is applicable at $T = 0$, can be found in Ref. [63].
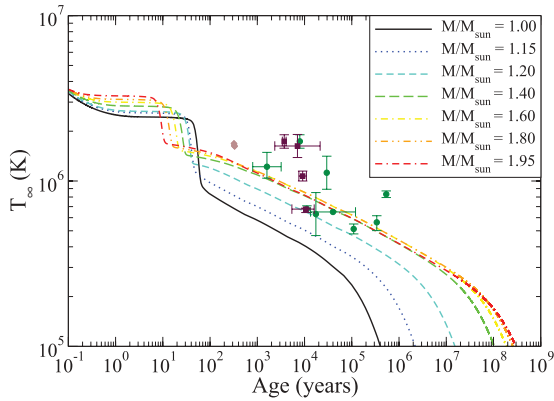
FIG. 6. (Color online) Thermal evolution of stars of different masses for model A. T_∞ denotes the redshifted temperature observed at infinity. The observed data consists of circles denoting spin-down ages, squares denoting kinematic ages, and diamonds denoting the Cas A evolution.

ages comparable with those of Cas A, it does not agree with the fast cooling exhibited by this object in the last 10 years. We point out, however, that differently than in Ref. [76] we have not removed fast neutrino emission processes by assuming that protons are in a superconducting state in the entire core. As pointed out in Ref. [78], such a stringent condition is more easily achieved for low density stars (less massive), since theoretical models show that proton superconductivity does not extend to very high densities. Under these conditions (no fast neutrino processes, and for the critical temperature found in Ref. [76]) our model might as well reproduce the observed behavior of Cas A.

The results shown in Fig. 6 clearly illustrate the effects of quark matter and the chiral partners on the cooling of the star, which we discuss now. The low density of the $M/M_\odot = 1.0$ star forbids the presence of chiral partners. Consequently the cooling of this object is qualitatively the same as that of standard hybrid stars [7]. On the other hand, for stars with higher central densities, and thus higher masses, we have chiral partner states being populated, and the cooling of the star is substantially modified. Note that these stars are warmer than their low-mass counterparts. Such behavior is the opposite of that of ordinary neutron stars, which tend to exhibit a faster
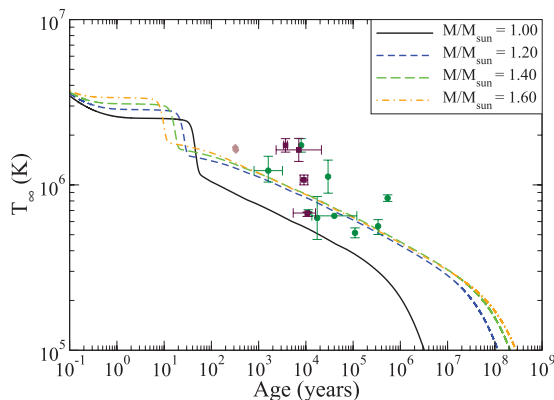

FIG. 7. (Color online) Same as Fig. 6 but for model B.

cooling for heavier objects. In the case of ordinary stars the acceleration of the cooling with the increase of density is connected to the increasing proton fraction. A higher proton fraction throughout the star means a larger region where the DU process is present, and thus a faster cooling. In our model, however, as the density increases (equivalent to smaller radius in Fig. 2) the proton fraction decreases due to the increase of the chiral partners population. Because of this, in our model, higher mass stars present a slower cooling. We also note that the cooling of stars in models A and B are qualitatively equal, with the difference that model B cannot reproduce stars with masses higher than $1.64 M_\odot$ (Fig. 7). Such an effect of slower cooling with increased mass has also been observed in hybrid stars with a color-superconducting quark core [80].

We should note here that these results should be considered with care. The reason is that so far we have not considered neutrino processes involving the chiral partners, which could certainly affect the cooling. The cross sections of the processes involving the chiral partners have not been determined so far, and are therefore excluded from this preliminary study. If one shows that those cross sections are much smaller than the ones of the traditional particles, i.e., the neutrino luminosity of this process is substantially smaller than that of the traditional DU process, then the results shown here would hold. These results can as well be easily tested, as soon as there is enough statistical data on the relation between pulsar age, surface temperature, and mass.

The results of Figs. 6 and 7 show that the cooling of hybrid stars in our model is considerably slower than that of traditional stars, even than that of the $M/M_\odot = 1.0$ star that does not contain chiral partners. Additionally, as we have already mentioned, we observe that during the neutrino dominated era (ages $\lesssim 10^4$ years in ordinary objects) more massive stars exhibit a higher temperature. This substantially delays the photon cooling era, that can be identified by the bending of the cooling tracks at later times. We see that our model, with the limitations discussed above, agrees fairly well with the cooling data of the colder and older objects, but fails to describe the temperature of the very young and hot neutron stars.

Another possibility to be considered is quark pairing. Our study considers a color-flavor-locked (CFL) [81] like phase, where all quarks of all colors are paired. Note that, since we consider small gap values only ($\Delta = 10$ MeV), which are not expected to substantially affect the equation of state (EoS) [82], we do not include corrections in the EOS. In this way, our analysis is still valid for any quark pairing scheme (not necessarily color superconductivity), as long as it affects all quark flavors in similar way. The quarks become a superconductor once the temperature falls below the critical temperature T_c. For this study we assumed, as in Ref. [73], the value of $T_c = 0.4\Delta$. Once the quarks become a superconductor the quark DU process is suppressed by a factor $e^{-\Delta/T}$, and the modified Urca and the Bremsstrahlung processes by a factor $e^{-2\Delta/T}$. The specific heat of quark matter is also modified by a factor $3.2(T_c/T) \times [2.5 - 1.7(T/T_c) + 3.6(T/T_c)^2]e^{-\Delta/T}$ [73].

We stress that the color-superconducting phase considered here is not, rigorously speaking, the traditional CFL phase. In
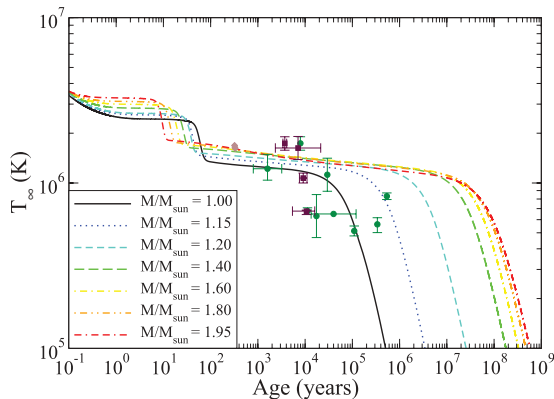
FIG. 8. (Color online) Same as in Fig. 6 but for quark matter paired with $\Delta = 10$ MeV.

the CFL phase, all quarks of all flavors are paired. On another hand, in the two-flavor superconducting state (2SC) one has the BCS pairing between u and d quarks of colors r and g, which leaves some cooling channels unsuppressed, thus leading to a faster cooling. Differently than the 2SC phase, the model we consider in our calculations assumes that u and d quarks of all colors are paired. As discussed above we consider only small gap values ($\Delta = 10$ MeV), which have little effect on the EoS. In that sense our pairing model is similar (but not exactly equal) to that discussed in Ref. [83], labeled 2SC+x, where we have a 2SC pairing of the u and d of two colors, and a residual pairing of the remaining unpaired quark, leading to the effective pairing of all u and d quarks.

We show in Fig. 8 and 9 the cooling of stars whose quark cores are in a superconductor state with $\Delta = 10$ MeV. One can see that the suppression of the quark emission processes allow the stars to be warmer during their neutrino cooling eras, in better agreement with the data of the very young and hot neutron stars. The time scale for the onset of the photon cooling era is unchanged. As was the case for stars with unpaired quark matter, the cooling of stars in models A and B are very similar. As was the case before, we stress that these results should be considered with great care, since the pairing scheme assumed here is phenomenological. A more detailed study,
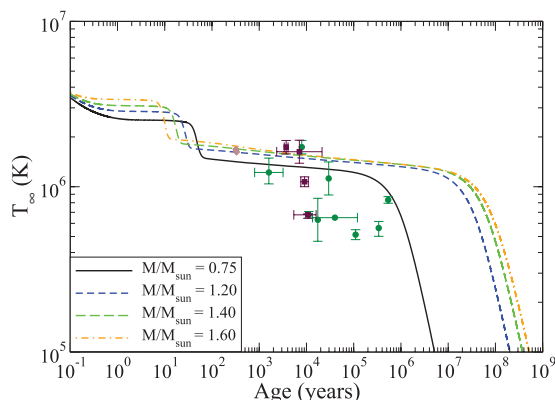

FIG. 9. (Color online) Same as in Fig. 7 but for quark matter paired with $\Delta = 10$ MeV.

taking into account microscopic effects, is warranted and will be performed in a future study.

VI. CONCLUSION

We applied for the first time the $SU(3)_f$ version of the parity doublet model to cold, dense, charge-neutral and chemically equilibrated matter. Note that this approach is able to successfully describe the low density as well as the high density regimes of the QCD phase diagram, as it includes a self-consistent deconfinement transition to quark matter. With these ingredients, we can study for the first time the interplay between the baryon octet, their respective chiral partners, and quarks in neutron stars. The chirally symmetric but still confined matter obtained in Ref. [20] disappears when charge neutrality and chemical equilibrium are taken into account. This is due to the early appearance of the down quark, that compensates the positive charge of the proton. Such a partial appearance of the quarks was already suggested in Ref. [84]. The up quark appearance happens, for both cold and warm stars, approximately in the same region as the chiral partners (signaling the chiral symmetry restoration).

The zero-temperature calculation using the same parametrization for the model as the one calibrated for low and zero chemical potential (model A) yields stars with masses in agreement with the most massive observed pulsar ($1.97 \pm 0.04 M_\odot$ [1]). This parametrization, however, leads to nuclear matter with high compressibility. On the other hand, parametrizations leading to more realistic compressibility values (such as model B) yield less massive stars. As already shown in Ref. [26], corrections that account for the baryonic Dirac sea effect, such as the relativistic Hartree approximation (RHA), can improve this situation. We note that the reason we did not consider any extra features that could possible improve the situation in this work is because we wanted to study in detail the population distribution in the star taking into account the relation between baryon chiral partners and quarks at high densities since this had never been performed before. Work along this line is in progress. The inclusion of finite temperature in the calculation allows more massive stars in both of the cases studied, but still does not qualitatively change the situation presented above.

We have performed cooling simulations for neutron stars whose microscopic composition is given by our (cold) model. We have found that the presence of the chiral partners affects the thermal evolution, effectively suppressing the hadronic direct Urca process. This, in contrast to other models, yields warmer stars during the neutrino cooling era, and delays the onset of the photon cooling era. Although we cannot effectively test such a prediction at the moment, we will be able to do so, hopefully, in the near future.

We also considered the possibility of pairing in the quark phase, where a CFL-like pairing was assumed. The suppression of the quark neutrino emission processes, brought on by pairing, reduces the total emission of neutrinos further, leading to even warmer stars in the neutrino cooling era. We stress that the cooling results presented here should be considered as a first approximation only, since there are many

factors that still need to be considered, such as the neutrino emissions from the chiral partners, and the effects of stronger quark pairing on the EoS, which warrants future work along those lines. We believe, however, that the cooling investigation put forth in this paper might be a good, qualitative study of the cooling of neutron stars within an $SU(3)_f$ doublet parity model composition, given that the available cooling data can be reproduced. Furthermore, a recent work [85] has shown that rotation might have an important effect on the cooling of compact stars, thus we intend to perform two-dimensional simulations of the thermal evolution of stars described by our model.

[1] P. Demorest, T. Pennucci, S. Ransom, M. Roberts, and J. Hessels, Nature (London) **467**, 1081 (2010).

[2] I. Vidana, D. Logoteta, C. Providencia, A. Polls, and I. Bombaci, Europhys. Lett. **94**, 11002 (2011).

[3] H. Chen, M. Baldo, G. F. Burgio, and H. J. Schulze, Phys. Rev. D **84**, 105023 (2011).

[4] S. Weissenborn, D. Chatterjee, and J. Schaffner-Bielich, Phys. Rev. C **85**, 065802 (2012).

[5] H. Ðapo, B. J. Schaefer, and J. Wambach, Phys. Rev. C **81**, 035803 (2010).

[6] D. L. Whittenbury, J. D. Carroll, A. W. Thomas, K. Tsushima, and J. R. Stone, arXiv:1204.2614.

[7] R. Negreiros, V. A. Dexheimer, and S. Schramm, Phys. Rev. C **85**, 035805 (2012).

[8] M. Alford, M. Braby, M. W. Paris, and S. Reddy, Astrophys. J. **629**, 969 (2005).

[9] S. Weissenborn, I. Sagert, G. Pagliara, M. Hempel, and J. Schaffner-Bielich, Astrophys. J. **740**, L14 (2011).

[10] L. Bonanno and A. Sedrakian, Astron. Astrophys. **539**, A16 (2012).

[11] J. Steinheimer and S. Schramm, Phys. Lett. B **696**, 257 (2011).

[12] T. Kunihiro, Phys. Lett. B **271**, 395 (1991).

[13] L. Ferroni and V. Koch, Phys. Rev. C **83**, 045205 (2011).

[14] Y. Aoki, G. Endrodi, Z. Fodor, S. D. Katz, and K. K. Szabo, Nature **443**, 675 (2006).

[15] S. Borsanyi *et al.*, J. High Energy Phys. 11 (2010) 077.

[16] A. Bazavov and P. Petreczky (HotQCD Collaboration), J. Phys. Conf. Ser. **230**, 012014 (2010).

[17] M. Fromm, J. Langelage, S. Lottini, M. Neuman, and O. Philipsen, arXiv:1207.3005.

[18] A. Ohnishi, H. Ueda, T. Z. Nakano, M. Ruggieri, and K. Sumiyoshi, Phys. Lett. B **704**, 284 (2011).

[19] G. Shen, C. J. Horowitz, and E. O'Connor, Phys. Rev. C **83**, 065808 (2011).

[20] J. Steinheimer, S. Schramm, and H. Stocker, Phys. Rev. C **84**, 045208 (2011).

[21] C. DeTar and T. Kunihiro, Phys. Rev. D **39**, 2805 (1989).

[22] T. Hatsuda and M. Prakash, Phys. Lett. B **224**, 11 (1989).

[23] Y. Nemoto, D. Jido, M. Oka, and A. Hosaka, Phys. Rev. D **57**, 4124 (1998).

[24] D. Jido, T. Hatsuda, and T. Kunihiro, Phys. Rev. Lett. **84**, 3252 (2000).

[25] V. Dexheimer, S. Schramm, and D. Zschiesche, Phys. Rev. C **77**, 025803 (2008).

[26] V. Dexheimer, G. Pagliara, L. Tolos, J. Schaffner-Bielich, and S. Schramm, Eur. Phys. J. A **38**, 105 (2008).

[27] C. Sasaki and I. Mishustin, Phys. Rev. C **82**, 035204 (2010).

[28] J. Steinheimer, V. Dexheimer, M. Bleicher, H. Petersen, S. Schramm, and H. Stöcker, Phys. Rev. C **81**, 044913 (2010).

[29] E. Santini, J. Steinheimer, M. Bleicher, and S. Schramm, Phys. Rev. C **84**, 014901 (2011).

[30] H. Petersen, Phys. Rev. C **84**, 034912 (2011).

[31] L. McLerran and R. D. Pisarski, Nucl. Phys. A **796**, 83 (2007).

[32] S. Lottini and G. Torrieri, Phys. Rev. Lett. **107**, 152301 (2011).

[33] L. Bonanno and F. Giacosa, Nucl. Phys. A **859**, 49 (2011).

[34] F. Giacosa, arXiv:1106.0523.

[35] D. Zschiesche, L. Tolos, J. Schaffner-Bielich, and R. D. Pisarski, Phys. Rev. C **75**, 055202 (2007).

[36] S. Gallas, F. Giacosa, and D. H. Rischke, Phys. Rev. D **82**, 014004 (2010).

[37] K. Fukushima and Y. Hidaka, Phys. Rev. D **75**, 036002 (2007).

[38] C. R. Allton *et al.*, Phys. Rev. D **66**, 074507 (2002).

[39] A. Dumitru, R. D. Pisarski, and D. Zschiesche, Phys. Rev. D **72**, 065008 (2005).

[40] C. Ratti, M. A. Thaler, and W. Weise, Phys. Rev. D **73**, 014019 (2006).

[41] K. Fukushima, Phys. Lett. B **591**, 277 (2004).

[42] G. Baym, C. Pethick, and P. Sutherland, Astrophys. J. **170**, 299 (1971).

[43] J. M. Lattimer and F. D. Swesty, Nucl. Phys. A **535**, 331 (1991).

[44] R. Hagedorn and J. Rafelski, Phys. Lett. B **97**, 136 (1980).

[45] J. Baacke, Acta Phys. Pol. B **8**, 625 (1977).

[46] M. I. Gorenstein, V. K. Petrov, and G. M. Zinovev, Phys. Lett. B **106**, 327 (1981).

[47] R. Hagedorn, Z. Phys. C **17**, 265 (1983).

[48] D. H. Rischke, M. I. Gorenstein, H. Stoecker, and W. Greiner, Z. Phys. C **51**, 485 (1991).

[49] J. Cleymans, M. I. Gorenstein, J. Stalnacke, and E. Suhonen, Phys. Scr. **48**, 277 (1993).

[50] J. I. Kapusta and K. A. Olive, Nucl. Phys. A **408**, 478 (1983).

[51] K. A. Bugaev, M. I. Gorenstein, H. Stoecker, and W. Greiner, Phys. Lett. B **485**, 121 (2000).

[52] K. A. Bugaev, Nucl. Phys. A **807**, 251 (2008).

[53] L. M. Satarov, M. N. Dmitriev, and I. N. Mishustin, Phys. At. Nucl. **72**, 1390 (2009).

[54] M. Hempel, J. Schaffner-Bielich, S. Typel, and G. Ropke, Phys. Rev. C **84**, 055804 (2011).

[55] H. Shen, H. Toki, K. Oyamatsu, and K. Sumiyoshi, Nucl. Phys. A **637**, 435 (1998).

[56] J. Steinheimer, S. Schramm, and H. Stocker, J. Phys. G **38**, 035001 (2011).

[57] P. Danielewicz, R. Lacey, and W. G. Lynch, Science **298**, 1592 (2002).

[58] J. M. Lattimer and Y. Lim, arXiv:1203.4286.

[59] R. C. Tolman, Phys. Rev. **55**, 364 (1939).

[60] J. R. Oppenheimer and G. M. Volkoff, Phys. Rev. **55**, 374 (1939).

[61] V. Dexheimer and S. Schramm, Astrophys. J. **683**, 943 (2008).

[62] V. Dexheimer, R. Negreiros, and S. Schramm, Eur. Phys. J. A **48**, 189 (2012).

[63] V. A. Dexheimer and S. Schramm, Phys. Rev. C **81**, 045201 (2010).

[64] F. Weber, *Pulsars As Astrophysical Laboratories for Nuclear and Particle Physics* (Institute of Physics, Bristol, 1999), p. 682.

[65] D. G. Yakovlev, A. D. Kaminker, O. Y. Gnedin, and P. Haensel, Phys. Rep. **354**, 1 (2001).

[66] N. Iwamoto, Ann. Phys. (NY) **141**, 1 (1982).

[67] D. Page, J. M. Lattimer, M. Prakash, and A. W. Steiner, Astrophys. J. Suppl. **155**, 623 (2004).

[68] E. Flowers and N. Itoh, Astrophys. J. **250**, 750 (1981).

[69] P. Haensel, Nucl. Phys. Proc. Suppl. B **24**, 23 (1991).

[70] E. H. Gudmundsson, C. J. Pethick, and R. I. Epstein, Astrophys. J. **259**, L19 (1982).

[71] E. H. Gudmundsson and C. J. Pethick, Astrophys. J. **272**, 286 (1983).

[72] D. Page, U. Geppert, and F. Weber, Nucl. Phys. A **777**, 497 (2006).

[73] D. Blaschke, T. Klahn, and D. N. Voskresensky, Astrophys. J. **533**, 406 (2000).

[74] K. P. Levenfish and D. G. Yakovlev, Astron. Lett. **20**, 43 (1994).

[75] C. Schaab, F. Weber, M. Weigel, and N. K. Glendenning, Nucl. Phys. A **605**, 531 (1996).

[76] D. Page, M. Prakash, J. M. Lattimer, and A. W. Steiner, Phys. Rev. Lett. **106**, 081101 (2011).

[77] P. S. Shternin, D. G. Yakovlev, C. O. Heinke, W. C. G. Ho, and D. J. Patnaude, Mon. Not. R. Astron. Soc. Lett. **412**, L108 (2011).

[78] D. Page, M. Prakash, J. M. Lattimer, and A. W. Steiner, arXiv:1110.5116.

[79] D. Page, J. M. Lattimer, M. Prakash, and A. W. Steiner, Astrophys. J. **707**, 1131 (2009).

[80] T. Noda, M. Hashimoto, Y. Matsuo, N. Yasutake, T. Maruyama, T. Tatsumi, and M. Fujimoto, arXiv:1109.1080.

[81] M. G. Alford, A. Schmitt, K. Rajagopal, and T. Schafer, Rev. Mod. Phys. **80**, 1455 (2008).

[82] M. G. Alford and S. Reddy, Phys. Rev. D **67**, 074024 (2003).

[83] D. Blaschke, D. Voskresensky, and H. Grigorian, Nucl. Phys. A **774**, 815 (2006).

[84] D. Blaschke, F. Sandin, T. Klahn, and J. Berdermann, in *Hadronic Physics: Joint Meeting Heidelberg-Liège-Paris-Wroclaw (HLPW 2008), March 2008, Spa, Belgium*, edited by J. Cugnon, L. Jean-Philippe, and N. Matagne, AIP Conf. Proc. No. 1038 (AIP, New York, 2008), p. 183.

[85] R. Negreiros, S. Schramm, and F. Weber, Phys. Rev. D **85**, 104019 (2012).